Published in final edited form as:
Biomaterials. 2012 December ; 33(36): 9167–9178. doi:10.1016/j.biomaterials.2012.09.009.

Electrospun Hydroxyapatite-Containing Chitosan Nanofibers Crosslinked with Genipin for Bone Tissue Engineering

Michael E. Frohbergh[1], **Anna Katsman, MD**[2], **Gregory P. Botta, PhD**[1,3], **Phillip Lazarovici, PhD**[1,4], **Caroline L. Schauer, PhD**[5], **Ulrike G. K. Wegst, PhD**[5,6], and **Peter I. Lelkes, PhD**[7,1,*]

[1]Drexel University, Philadelphia, PA, School of Biomedical Engineering, Science and Health Systems

[2]Drexel University College of Medicine, Department of Orthopedic Surgery

[3]Drexel University College of Medicine, Molecular and Cellular Biology & Genetics

[4]Hebrew University of Jerusalem, Israel – Institute for Drug Research

[5]Drexel University, College of Engineering, Department of Materials Science and Engineering

Abstract

Reconstruction of large bone defects remains problematic in orthopedic and craniofacial clinical practice. Autografts are limited in supply and are associated with donor site morbidity while other materials show poor integration with the host's own bone. This lack of integration is often due to the absence of periosteum, the outer layer of bone that contains osteoprogenitor cells and is critical for the growth and remodeling of bone tissue. In this study we developed a one-step platform to electrospin nanofibrous scaffolds from chitosan, which also contain hydroxyapatite nanoparticles and are crosslinked with genipin. We hypothesized that the resulting composite scaffolds represent a microenvironment that emulates the physical, mineralized structure and mechanical properties of non-weight bearing bone extracellular matrix while promoting osteoblast differentiation and maturation similar to the periosteum. The ultrastructure and physicochemical properties of the scaffolds were studied using scanning electron microscopy and spectroscopic techniques. The average fiber diameters of the electrospun scaffolds were 227±154 nm as spun, and increased to 335±119 nm after crosslinking with genipin. Analysis by X-ray diffraction, Fourier transformed infrared spectroscopy and energy dispersive spectroscopy confirmed the presence of characteristic

Corresponding Author: Peter I. Lelkes, Department of Bioengineering, Temple University, Engineering Building Room 413, 2147 North 12th Street, Philadelphia PA, 19122, Tel: 215-204-3307, pilelkes@temple.edu.
[6]current address: Dartmouth College, Hanover, NH, Thayer School of Engineering
[7]current address: Temple University, Philadelphia, PA, Department of Bioengineering, College of Engineering
Co-Authors
Michael E. Frohbergh, School of Biomedical Engineering, Science and Health Systems, Drexel University, Mike Frohbergh <mikefro15@gmail.com>
Anna Katsman, Department of Orthopedic Surgery, Drexel University College of Medicine, Anya Katsman <anya1221@gmail.com>
Gregory P. Botta, Department of Biochemistry and Molecular Biology, Drexel University College of Medicine, Gregory Botta <gregory.botta@gmail.com>
Philip Lazarovici, Institute for Drug Research, Hebrew University, Jerusalem Israel, Philip Lazarovici <philipl@ekmd.huji.ac.il>
Caroline L Schauer, Department of Materials Science and Engineering, Drexel University, Caroline Schauer <cschauer@coe.drexel.edu>
Ulrike G.K. Wegst, Thayer School of Engineering, Dartmouth College, Ulrike Wegst Ulrike.Wegst@dartmouth.edu

Author's Disclosure Statement: No competing financial interests exist

features of hydroxyapatite in the composite chitosan fibers. The Young's modulus of the composite fibrous scaffolds was 142±13 MPa, which is similar to that of the natural periosteum. Both pure chitosan scaffolds and composite hydroxyapatite-containing chitosan scaffolds supported adhesion, proliferation and osteogenic differentiation of mouse 7F2 osteoblast-like cells. Expression and enzymatic activity of alkaline phosphatase, an early osteogenic marker, were higher in cells cultured on the composite scaffolds as compared to pure chitosan scaffolds, reaching a significant, 2.4 fold, difference by day 14 ($p<0.05$). Similarly, cells cultured on hydroxyapatite-containing scaffolds had the highest rate of osteonectin mRNA expression over 2 weeks, indicating enhanced osteoinductivity of the composite scaffolds. Our results suggest that crosslinking electrospun hydroxyapatite-containing chitosan with genipin yields bio-composite scaffolds, which combine non-weight-bearing bone mechanical properties with a periosteum-like environment and facilitate the proliferation, differentiation and maturation of osteoblast-like cells. We propose that these scaffolds might be useful for the repair and regeneration of maxillofacial defects and injuries.

Keywords

Chitosan; hydroxyapatite; genipin; electrospinning; bone tissue engineering; osteoblast differentiation

1. INTRODUCTION

Reconstruction of large bone defects formed as a result of trauma, resection, or congenital malformations remains problematic in orthopedic and craniofacial clinical practice. With the goal of shifting the strategy from prosthetic replacement to regeneration, bone tissue engineering using osteo-inductive and -conductive scaffolds may offer an alternative approach to overcome this problem.

Currently, a variety of methods, including autografts, allografts, and alloplastic materials are used for treatment of such defects. Each of the strategies, however, has significant drawbacks. While the gold standard, autografts, are limited in supply and are associated with donor site morbidity, allografts and prosthetic materials often show poor integration with the surrounding host bone, fragmentation, and displacement [1–3]. Bone is a unique triphasic tissue that contains cellular components, hydrated extracellular organic matrix, and an extracellular mineral phase, which is mainly composed of calcium phosphate in the form of hydroxyapatite (HA) [4–6]. The outer layer, the periosteum, harbors multipotent mesenchymal stem cells and osteoprogenitor cells that contribute to growth and regeneration of bone [7]. It has been reported that mechanical properties at the interface between the graft and the host tissue remain impaired when compared to autografts due to the lack of new bone formation around this junction [8]. Thus, engineering a bioactive scaffold that combines the organic-inorganic interphase of bone tissue with the regenerative capacity of the periosteum may be a potential solution to the lack of osseointegration of autograft substitutes.

Since an optimal bone substitute integrating these features still remains to be identified, a wide array of fabrication techniques and materials has been proposed to create biomimetic scaffolds that would aid in bone regeneration. One such platform technology is electrospinning, an established textile manufacturing technique that can be used to generate non-woven fibrous scaffolds with fiber diameters ranging from nano- to micrometers[9]. Nanofibrous architecture may be beneficial in terms of the proliferation, differentiation, and mineralization of osteoprogenitor cells [10]. Co-electrospinning, i.e. combining polymers with bioactive substances such as HA, can further improve the biomimetic properties of

nanofibrous scaffolds and enhance cell attachment, osteoblastic differentiation, and bone extracellular cell matrix (ECM) synthesis [11–13]. Chitosan (CTS) [14–16], the deacetylated form of chitin, a polysaccharide derived from the exoskeleton of crustaceans [17] has emerged as a promising candidate for bone tissue engineering, mainly due to its biocompatibility and structural similarity to bone ECM [18, 19]. Recent approaches focus on co-electrospinning CTS with other materials, such as collagen, poly(lactic-co-glycolic acid) (PLGA) and poly(caprolactone) (PCL) for a variety of applications, including that of engineering functional bone scaffolds [13, 20–24]. However, little attention has been paid to generating fibrous chitosan-based scaffolds which combine the physical properties of cortical bone and the mechanical and conductive properties of the periosteum, the layer of bone that is responsible for the success of autografts over allografts and engineered constructs [8]. We hypothesize that electrospun chitosan-hydroxyapatite bio-composites in conjunction with bone progenitor cells might serve as bioactive tissue-engineered bone scaffolds by mimicking the mechanical properties and regenerative capacity of periosteum while facilitating osteoblast migration from the scaffold/tissue interface. Moreover, by mimicking the architectural structure of mature bone, these composite scaffolds will also enhance the differentiative capacity and ECM deposition of osteogenic precursor cells, acting as a bio-template upon which new bone can be formed.

Tunable mechanical properties are of particular importance when fabricating tissue-specific scaffolds. Alterations in mechanical properties of natural and synthetic biomaterials can be introduced by physical, enzymatic, or chemical crosslinking [25–27]. Genipin (GP) is a non-toxic, natural crosslinker that is derived from the fruit of gardenia extracts. It has been proposed that GP binds to the free amine groups on the outside of fibrous polymer chains, e.g., in a silk fibroin-hydroxybutyl chitosan hybrid scaffold, forming new bonds between the fibers and thus increasing the stiffness of GP-crosslinked engineered scaffolds [28]. Although crosslinking CTS with GP has been proposed to increase the stiffness of hydrogels used for soft tissue engineering [29], this approach has been considered only recently for bone engineering [30, 31] and has not yet been reported for CTS-HA composite scaffolds.

In this study we analyzed the effects of HA and genipin crosslinking on the mechanical properties of the electrospun chitosan scaffolds and explored the effects of hydroxyapatite nanoparticles on the adhesion, proliferation, and maturation/differentiation of murine 7F2 osteoblast-like bone precursor cells.

2. MATERIALS AND METHODS

2.1 Materials

Medium molecular weight chitosan (CTS, 75% – 85% deacetylated), trifluoroacetic acid (TFA, ≥98%), and hydroxyapatite (HA, reagent grade, <200 nm nanoparticles) were purchased from Sigma-Aldrich Co. Ltd. (St. Louis, MO). Genipin (GP, ≥98% pure) was from Wako Pure Chemical Industries Ltd. (Osaka, Japan). The alamar blue colorimetric assay kit was purchased from AbD Serotec (Raleigh, NC). The alkaline phosphatase colorimetric assay was purchased from Abcam (Cambridge, MA). All PCR kits and master mixes were purchased from Qiagen (Valencia, CA) and all primers from Applied Biosystems (Carlsbad, CA).

2.2 Electrospinning

Scaffolds were electrospun from a solution of CTS dissolved in TFA to yield 7% (w/v) CTS. HA-containing scaffolds were generated by admixing 0.8%, 1.0% or 2.0% HA nanoparticles (w/v) to the CTS solution. All solutions were stirred at room temperature for at least 5 days. Electrospinning was performed in a homemade system, essentially as previously described

[16, 32]. In brief, 5 mL glass syringes (BD, multifit syringes) containing 4 ml each of the above solutions were mounted in a KDS200 syringe pump (KD Scientific). The flow rate was set to 1.2 ml/hr. A voltage of 15 kV between the syringe tip and the target, generated by an ES-30 Gamma High Voltage Research power supply (Gamma High Voltage Research), was applied by connecting the cathode to the syringe needle and the anode to a rectangular 6 × 2 cm aluminum collecting plate placed 15 cm from the tip of the needle.

2.3 Crosslinking

Electrospun scaffolds were crosslinked with 0.1 % (w/v) GP. The scaffolds were first stabilized ("waterproofed") by soaking them for 20 minutes in 0.5% sodium hydroxide (NaOH) dissolved in 100% ethanol, followed by five 30 second washes with 1X phosphate buffer solution (PBS) to remove any trace amounts of ethanol [33]. The stabilized scaffolds were then crosslinked in 0.1% (w/v) genipin dissolved in 1X PBS for 24 hours. The crosslinking process was terminated by washing the scaffolds in PBS, as described above. The resulting scaffolds were termed chitosan-genipin crosslinked scaffolds (CTS-GP) or chitosan-hydroxyapatite-genipin crosslinked composite scaffolds (CTS-HA-GP).

2.4 Scaffold Characterization

2.4.1 Scanning Electron Microscopy—For ultrastructural analysis, circular scaffold samples of 10.3 mm diameter were sputter coated with carbon. The samples were viewed and digitally photographed in a Zeiss Supra50VP field emission scanning electron microscope (FESEM) equipped with an Oxford Instruments INCA Energy Dispersive Spectrometer at 5 kV with the SE2 detector using a 30 μm final aperture.

2.4.2 Electron Dispersive X-ray Spectroscopy (EDS)—An FESEM equipped with an EDAX electron dispersive X-ray spectroscopy system and was used to assess calcium and phosphorous contents of the scaffolds. X-ray spectra were taken at 10 kV using a 60 μm final aperture. EDS was performed using the FESEM at an acceleration voltage of 10 kV.

2.4.3 X-ray Diffraction (XRD)—XRD was performed using a Siemens D500 powder diffractometer using conventional Bragg–Brentano geometry in q – 2q configuration, with Cu_{Ka} source (l = 0.154 nm). 2q scans were acquired from 10 – 60° with a step of 0.03° and 1s dwell time per point.

2.4.4 Fourier Transform Infrared Spectroscopy (FTIR)—FTIR spectra were collected on a Varian Inc. FTS3000 Excalibur FTIR spectrometer equipped with a Deuterated Triglycine Sulfate (DTGS) detector and KBr beam splitter. The spectra were recorded at resolution of $4cm^{-1}$ in transmission mode.

2.4.5 Mechanical Properties—The mechanical properties of the scaffolds were tested using the Instron 5564 Table Mounted Materials Testing System and Merlin Series IX software (Instron, Norwood, MA). Hydrated CTS-GP and CTS-HA-GP scaffolds were cut into strips of 22.7 ± 2.3 mm × 5.4 ± 0.7 mm (n = 28). Samples were prepared by either waterproofing CTS-HA-GP scaffolds and then washing 5 times in 1X PBS or by waterproofing followed by crosslinking in 0.1% GP for 24 hours and then washing 5 times with 1X PBS. All samples were stored in 100 mm petri dishes containing 1X PBS until testing. To simulate a "biologic" environment, samples were tested under wet conditions immediately upon removal from the PBS. A gauge length of 10 mm was used for all samples. The strain rate was set at 1 mm/min. The Young's modulus was calculated from the linear portion of stress-strain curves. The ultimate tensile strength (UTS) was determined by calculating the stress at break normalized to the cross-sectional area of the scaffold. The measured average thickness of the scaffolds was 25.3 ± 16.2 μm (n = 28).

2.5 Cell Culture

Murine 7F2 osteoblast-like cells were obtained from ATCC and cultured in alpha modification of Minimum Essential Medium (α-MEM) containing 1 g/L glucose, 10% fetal bovine serum (FBS), 2 mM L-glutamine, 1% (v/v) penicillin-streptomycin. Cells were placed within T-cell culture flasks in an incubator set to 37°C and 5% carbon dioxide. The medium was changed every second day. The cells were passaged three times by trypsinization prior to seeding onto the scaffolds, as described below.

2.6 Seeding of 7F2 cells on scaffolds

Circular scaffolds with a diameter of 10.3 mm, cut from either the CTS-HA-GP (1.0% HA) or CTS-GP electrospun sheets, were placed in 24 well plates, secured with a Viton O-ring [34], stabilized, and crosslinked with 0.1% GP, as described above. The samples were sterilized with UV light for one hour and pre-treated by soaking in complete medium overnight. 7F2 cells were seeded in aliquots of 50 μl containing 10,000 cells by carefully pipetting onto the center of the scaffold. The cell–seeded scaffolds were then placed into an incubator for one hour. After this time period, 450 μL of medium consisting of low glucose (1 g/L) α-MEM, 10% FBS, 2mM L-glutamine and 1% (v/v) penicillin-streptomycin was added to each well. The cells were cultured for up to 21 days during which time the medium was changed every other day. Cells were also cultured in a similar manner on tissue culture polystyrene (TCP) as a negative control.

2.7 Scanning electron microscopy (SEM)

To evaluate the morphology of cells growing on the scaffolds, samples were fixed on days 7, 14 or 21 post-seeding, as above, and serially dehydrated in ethanol and hexamethyldisilazane (HMDS) for 10 minutes in each concentration as previously described [35]. The samples were left to air dry in a chemical fume hood overnight at room temperature, sputter coated with carbon, and observed under SEM, as described above. Attempts at critical point drying the samples were abandoned, since CPD significantly reduced the sizes of the scaffold to a point that they were unusable.

2.8 Cell Viability and Proliferation

Cell viability and proliferation were continually monitored over a 21 day period using the continual alamarBlue™ (AB) assay on days 0, 3, 7, 14 and 21 as previously described [36]. In brief, 7F2 cells were seeded in 24 well plates onto TCP as well as onto circular CTS-GP and CTS-HA-GP scaffolds at a density of 3.5×10^4 cells/well. At the time points stated above, AB was added at 10% (v/v) in triplicate to each well. The plates were then returned to the incubator for three hours. For zero control, AB was also either added to wells containing only medium or scaffolds and media. After 3 hours, 200 μl aliquots of the supernatant were pipetted in triplicate into 96 well plates and the AB fluorescence was read in a Synergy 4 microplate reader (Biotek, Winooski, VT) at an excitation wavelength of 545 nm and an emission wavelength of 590 nm. The data were analyzed using Gen5 software (Biotek) and samples were normalized to their respective zero controls. The cells were re-fed with fresh medium and placed in the incubator to be analyzed at the next time point.

2.9 Alkaline Phosphatase (ALP) Activity Assay

ALP is an early marker for differentiation towards the osteocytic phenotype [20]. Murine 7F2 osteoblast-like cells were seeded, on TCP, CTS-GP and CTS-HA-GP scaffolds in 24 well plates at a density of 3.5×10^4 cells/well. ALP activity was measured colorimetrically on days 0, 7, 14 and 21 using a commercial kit (Abcam, ab83369). At each time point, three cell-seeded scaffolds were homogenized in a glass tube homogenizer containing 300 μL of lysis buffer (kit component). The supernatant was collected and centrifuged at 1350 rpm for

3 minutes to remove all insoluble debris. 30 μL aliquots of the resultant samples were added to a 96 well plate followed by 50 μL of assay buffer and 50 μL of *para*-Nitrophenylphosphate (pNPP) solution. Following incubation for one hour at room temperature, 20 μL of stop buffer was added to the samples and the absorbance was read in the microplate reader at 420 nm, as described above. To assess the ALP activity of control cells growing on TCP, the wells were rinsed with 300 μL of 1X PBS, followed by addition of 1X lysis buffer for 10 minutes. After that, the supernatant was collected and cell remnants were scraped with a cell scraper for manual lysis. The protocol for analyzing ALP activity was then followed, as above.

2.10 RNA Isolation and quantitative real time RT-PCR

7F2 cells were trypsinized after 7, 14 or 21 days of culture on TCP, CTS-GP and CTS-HA-GP scaffolds. The cells were pelleted by centrifugation at 800 RPM for 5 minutes. After a 1X PBS wash, the resulting pellet was stored at −80 °C prior to RNA isolation. A Qiagen RNeasy Mini Kit was used to isolate RNA by columnar centrifugation and DNase digestion, as per the manufacturer's instructions. RNA integrity was initially determined by electrophoresis on 1.0% agarose gels. Quantitative real-time reverse transcription polymerase chain reaction (qRT-PCR) was performed with a Qiagen One-Step Kit combined with TaqMan expression assays according to the manufacturer's instructions. qRT-PCR was performed using a Realplex II thermal cycler (Eppendorf, Hamburg, Germany) using the following Taqman primers (from Applied Biosystems, Carlsbad, CA): Spock (Osteonectin, Mm00486393_m1), Alkaline Phosphatase (Mm01187115_m1), Spp1 (Osteopontin, Mm00436767_m1). GAPDH (Hs99999905_m1) was used as an internal 'housekeeping' control. Primer efficiency was determined by linear regression of a dilution series. Cycle threshold (CT) results were analyzed by the Pfaffl Method. The results were normalized to TCP and GAPDH prior to logarithmic transformation [37]. Each experimental condition and gene primer was analyzed in triplicate.

2.11 Statistical Analysis

Unless stated otherwise, all experiments were repeated independently at least three times in triplicate. All data are presented as mean values ± standard deviation. Results were analyzed using a one-way ANOVA test of variance with an ad hoc Tukey Test. Results with p-values of < 0.05 (*) and 0.01 (**) were considered statistically significant.

3. RESULTS

3.1 Morphology of Genipin crosslinked chitosan/hydroxyapatite nanofibers

Optimization of the electrospinning process for generating pure chitosan (CTS) and chitosan-hydroxyapatite (CTS-HA) fibers was required because most current processes use fiber-forming high molecular weight additives, such as poly(ethylene oxide) (PEO), which can inhibit multi-layer growth of cells [38]. Initial optimization included systematically adjusting the solute concentration, flow rate, working distance and voltage of the electrospinning platform, as previously described [32, 39–41], to yield electrospun fibers that were continuous, uniform in shape and without beading. The measured thickness of a typical, optimized, electrospun nanofibrous scaffold mat, such as shown in Figure 1A, was 25.3 ± 16.2 μm (n = 28, Figure 1B). The diameters of the individual non-crosslinked fibers in the mat, as evaluated by SEM, were on the average 227.8± 154.3nm (n=10 independent samples, analyzing ~50 fibers/sample). Crosslinking and hydration caused an increase in the diameter of the fibers to 334.7 ± 119.1 nm (n=10 independent samples, analyzing ~ 50 fibers/sample). In contrast to the smooth surface of CTS-GP fibers (Figure 2A), CTS-HA-GP fibers contained nanoparticles dispersed on the surface (Figures 2B).

3.2 Evaluation of Nanoparticle Deposits on CTS-HA-GP nanofibers

Three independent approaches, X-ray diffraction (XRD), Fourier transform infrared spectroscopy (FTIR) and energy dispersive X-ray spectroscopy (EDS), were employed to further characterize the chitosan scaffolds, specifically the nanoparticle deposits observed on the surface of the CTS-HA-GP nanofibers [19]. XRD spectroscopy shows the characteristic, highly crystalline structure for the pure HA powder, while the spectrum of CTS-GP scaffolds resembled that of amorphous electrospun CTS (Figures 3A and B). The spectra for the CTS-HA-GP composite fibers containing nanoparticles revealed three distinct peaks at 26.21, 30.24 and 32.41 degrees corresponding to HA. These new peaks indicate introduction of crystalline properties into the amorphous nanostructure of the CTS-GP scaffolds due to the presence of HA and, therefore, indicate the formation of a biocomposite material (Figure 3C). The phosphate groups in pure HA showed characteristic FTIR bands between 900–1100cm^{-1} and 500–600cm^{-1}(Figure 4A) [19]. FTIR Spectra of the CTS-HA-GP bio-composites revealed bands at 500–600cm^{-1} that did not appear in the CTS-GP scaffold spectra (Figures 4B and C). Additionally, there was a broadening of the band around 950cm^{-1} and 1085cm^{-1} that appeared on the CTS-HA-GP spectra, which has been attributed to the interaction of HA and chitosan (Figure 4C) [19]. Finally, EDS was used to determine the elemental composition of the individual nanofibers. CTS-GP scaffolds showed large peaks for carbon and oxygen and a small peak for nitrogen, indicating three of the main components of chitosan (Figure 5A). Fibers containing1.0% HA, additionally contained small amounts of calcium and phosphorus (insert in Figure 5A). The peaks for 0.8% HA containing fibers were somewhat smaller, indicating that less HA had been incorporated, while at 2.0% HA the peaks were similar to those at 1.0%, indicating saturation (data not shown). Elemental analysis of the EDS intensity maps showed the distribution of carbon (Figure 5B) and oxygen (Figure 5C) as the main organic components of the fibers, while inorganic calcium (Figure 5D) and phosphate were found (Figure 5E) in the form of HA nanoparticles on each fiber (Figures 5B, C, D, and E, respectively).

3.3 Mechanical Properties of CTS-HA-GP nanofibers

The effect of HA on the mechanical properties of genipin crosslinked scaffolds was tested using three different concentrations of HA. As seen in the top panel of Figure 6, crosslinking with genipin increased the ultimate tensile strength (UTS), as determined by the stress at break normalized to the cross-sectional area of the scaffold, by approximately 50% when compared to the non-crosslinked scaffolds, however there was no significant difference between the UTS values, when the concentration of HA was increased from 0.8% – 2.0%. Increasing the HA concentration from 0.8%, 1.0%, and 2.0% increased the Young's moduli of non-crosslinked CTS-HA scaffolds significantly from 0.8% to 1.0% ($p < 0.05$), with no increase when the HA concentration was raised from 1.0% to 2.0% (Figure 6, bottom panel). Crosslinking with GP resulted in a significant increase in the Young's moduli to 77.2±8.6 to 142.5±12.5 and 147.4±21.7 MPa for samples containing 0.8%, 1.0% and 2.0% HA, respectively. These measurements indicate a 4–5 fold increase ($p < 0.01$) in stiffness for all crosslinked samples over that of non-crosslinked samples (Figure 6, bottom panel, $n = 6$ scaffolds per condition). Like in the case of the UTS, there was a significant increase in the stiffness when the HA concentration was raised from 0.8% to 1.0% after crosslinking ($p < 0.01$) with no further increase when increasing the HA =concentration to 2.0%. These results are comparable to the EDS results, indicating a saturation of HA on the scaffolds at 1.0%.

3.4 Morphology of 7F2 osteoblasts on CTS-HA-GP Scaffolds

The morphology of the cells cultured on CTS-GP and CTS-HA-GP nanofibers was evaluated by SEM. At seven days post-seeding, cells formed extensive cell-scaffold and cell-cell interactions indicative of cellular proliferation/migration and cell-cell and cell-scaffold interactions, as inferred from the well-defined filopodia extending from the

lamellipodia and “grabbing” the nanofibers on both CTS-GP and CTS-HA-GP scaffolds. The cells were observed for up to 21 days. By day 14, much more confluent monolayers were spread on the scaffold, indicating continued proliferation (Figure 7A and C). Noticeable on day 14 was the presence of a rougher texture on the CTS-HA-GP scaffolds (Figure 7A and B) than on the CTS-GP scaffolds (Figure 7C and D), indicating an enhanced maturation of 7F2 cells by the presence of a mineralized ECM deposition. This morphology was maintained on CTS-HA-GP scaffolds up to 21 days and the rough texture was also observed on CTS-GP scaffolds on day 21, indicating the eventual maturation and mineralized ECM deposition.(data not shown)

3.5 Capacity of CTS-HA-GP Scaffolds to Induce Osteogenic Differentiation in vitro

Upon osteogenic differentiation, 7F2 pre-osteoblastic cells, secrete alkaline phosphatase (ALP) and mineralize their own matrix [42]. The osteoinductive potential of the scaffolds was determined by measuring the activity of ALP, an early osteogenic marker, using a colorimetric pNPP assay on days 7, 14, and 21 post-seeding (Figure 8A). When grown on tissue culture plastic (TCP), 7F2 cells had low ALP activity that remained stable over a 21 day period and was consistently lower than when grown on the cross-linked CTS-GP scaffolds ($p < 0.01$). By day 14, ALP activity in cells growing on the CTS-HA-GP bio-composite scaffolds was 2.4 fold higher than on CTS-GP scaffolds ($p < 0.01$). Expression of this early osteogenic marker decreased on both scaffolds by day 21 as differentiation continued and cells matured. Cell metabolic activity was assessed continually using the alamarBlue™ (AB) assay. As seen in Figure 8B, the metabolic activity increased in all samples after 3 days. On TCP, AB fluorescence continued to increase over 21 days, while CTS-GP samples remained stable and CTS-HA-GP bio-composite samples decreased (Figure 8B). Cells cultured on TCP had the highest AB fluorescence at all time points, indicating maximal metabolic activity and, presumably, a minimal degree of differentiation. After an initial increase, the AB fluorescence of cells on CTS-HA scaffolds remained relatively stable over the experimental time course, suggesting a decrease in metabolic activity compared to TCP. This AB stability may also indicate that the cells are undergoing differentiation. Lastly, AB fluorescence on CTS-HA-GP composite nanofibers decreased over time, which may indicate enhanced differentiation in comparison to the CTS-HA scaffolds.

Early and late markers of osteogenic differentiation were assessed by qRT-PCR, measuring RNA expression of osteopontin (OP) and osteonectin (ON), respectively. As seen in Figures 8C and D, the expression of OP, an early marker of osteogenic differentiation is highest 24 hours after cell seeding and then decreases progressively at days 14 and 21 on both the CTS-GP and CTS-HA-GP composite scaffolds. By contrast, the mRNA expression of ON, which is a late marker of osteogenic maturation, was at its lowest levels at 24 hours and increased on days 14 and 21 in cells growing on the CTS-GP. However, on the CTS-HA-GP scaffolds, a significantly larger increase (by ~2 orders of magnitude) in ON expression, a marker of late osteogenic differentiation, between 24 hours and day 14 (with a subsequent plateau at day 21) was noticed when compared to the CTS-GP scaffolds. These data indicate that the presence of HA accelerated/enhanced osteogenic differentiation/maturation of 7F2 cells. This was further clarified by a similar trend in the decrease of OP, a marker of early osteogenic differentiation, on the mineralized scaffolds between 24 hours and 14 days on the CTS-HA-GP scaffolds with respect to CTS-GP scaffolds.

4. DISCUSSION

Repair of large bone defects remains a challenge in clinical practice and has spurned considerable reconstructive efforts by bone tissue engineering. The relative success of autografts in the repair of craniofacial defects has been ascribed to the recruitment of stem

cells by functional periosteum [8]. Periosteum, the thin fibrous layer surrounding bone, harbors mesenchymal progenitor cells whose recruitment, activation, and osteogenic differentiation is essential for bone graft integration, healing and remodeling [43]. By blocking fibrotic infiltration, the periosteum can beneficially promote the movement of osteoblasts across an allograft's surface while inducing their differentiation and proliferation [8]. Unlike autografts, however, allografts and other bone substitutes transplanted without this layer are, at best, osteoconductive. Our aim was to generate an allogeneic template scaffold that has the potential to act as a "bridge" on the periosteal interface of non-load bearing bone defects to induce osteogenic migration and self-regeneration. In this study, we evaluated the physicochemical characteristics of such scaffolds as well as their ability to promote adhesion, proliferation and osteogenic differentiation of osteoblast-like 7F2 cells.

Ideally, an engineered allogeneic bone scaffold will architecturally resemble bone matrix and have mechanical properties suitable for non-weight bearing, such as the repair of calvaria or similar craniofacial bones. Several two-step electrospinning processes have been described in the past for the formation of hydroxyapatite (HA) containing nanofibers by co-precipitating an HA solution and a polymer of interest, such as chitosan [20, 44]. In this study we developed a simpler, one-step solution, in which we dissolved chitosan (CTS) and dispersed HA in trifluoroacetic acid (TFA) to create a homogenous, electrospinnable solution/dispersion. While CTS completely dissolved in TFA, HA did not, as inferred from the turbid appearance of the solution containing HA versus the clear solution without it. However, the homogenous dispersion of HA nanoparticles in TFA did permit the formation of CTS fibers which incorporated HA nanoparticles on the surface of composite fibers (Figure 2). Furthermore, by increasing the concentration of CTS from 2.7% to 7%, we were able to increase the previously reported thickness of the scaffolds by ~2 fold, from 10.1 ± 5.8 μm to 25.3 ± 16.2 μm [45].

As another innovation, we were able to electrospin CTS nanofibers without the use of a fiber-forming agents (FFAs), such as polyethylene oxide (PEO), which is often used to enhance chain entanglement of materials that do not have high electrospinnability [14, 20]. Past studies have indicated a need for FFAs, such PEO, in the case of electrospun soy-protein-isolate (SPI) solutions that could not form continuous fibrous meshes without an FFA [46]. SPI is a "green" material derived from the soy plant that is currently being evaluated as a potential scaffold for wound dressings [46]. As a caveat, it has been reported that inclusion of FFAs into a scaffold may delay or reduce cell adhesion, proliferation and/or differentiation due to their inherent nature in inhibiting protein adsorption [18].

Although a number of recent papers discuss electrospinning of CTS [16, 26, 45, 47, 48], there were numerous experimental parameters factors that needed to be optimized before we were able to obtain bead-free continuous CTS fibers. There is a wide divergence in the published literature regarding many of these parameters, such as concentrations of CTS and solvents used. Some of these inconsistencies may be due to the stringent requirements for controlling critical electrospinning CTS parameters, including humidity, temperature and % deacetylation. For our studies we worked in a controlled environment, e.g. lowering the humidity (~30% humidity vs. 50–60% as in a regular laboratory environment), keeping the ambient temperature around 20° – 22°C, and used a CTS with a degree of deacetylation that was 75%–85%. In our experience, the combination of these parameters proved to be critical for producing bead-free, smooth and continuous at a concentration of 7% CTS in TFA.

To evaluate the topography, structure, and fiber composition of HA containing electrospun scaffolds, we used 4 independent material characterization techniques (SEM, XRD, FTIR, and EDS). Analysis of SEM micrographs (Figure 2), revealed a mean fiber diameter of 335±119 nm for CTS-GP scaffolds. This large variability and heterogeneity in the size of

electrospun CTS nanofibers has been described before and may be due to inhomogeneity of the solution [24, 28, 49]. CTS has an extremely high surface tension and requires harsh solvents, such as TFA for appropriate fiber formation upon electrospinning [45]. We surmise that the large variability in fiber diameter we observed may be caused by the harsh solvents and/or conditions required to electrospin chitosan without and FFA.

EDS characterization ascertained that the nanofibers electrospun from the CTS containing 1.0% HA solution contained small amounts of calcium and phosphorous. The EDS peaks seen in Figure 5A show the presence of the main elemental components of chitosan: carbon, oxygen and nitrogen. Additionally, smaller phosphorous and calcium peaks are detected in the CTS-HA-GP scaffolds (Figure 5A, insert). To confirm the identities of the nanoparticles seen on the fibers, elemental analysis was performed. Carbon and oxygen (Figs. 5B and C), represented as white dots, make up the main components of the nanofibers, while smaller amounts of calcium and phosphorous (Figs. 5D and E) are dispersed amongst the carbon and oxygen. Heinemann et al. (2008) used qualitative EDS to determine the presence of calcium and phosphorous on collagen-coated chitosan scaffolds after seeding with 7F2 cells and concluded that the presence of these elements indicated mineralized matrix deposition from the 7F2 cells [50].

The XRD spectra of the bio-composite HA/chitosan scaffolds show distinct peaks that specifically match those found in pure HA samples (Figure 3). The peaks in the CTS-HA-GP spectra are an indication of semi-crystalline HA structures present in the composites as opposed to the completely amorphous nature of CTS-GP scaffolds. As additional evidence for the presence of HA in composite scaffolds, molecular interactions and vibrations in the CTS-HA-GP scaffolds were analyzed by FTIR. While calcium is vibrationally "undetectable," some small bands between 1000–1100cm^{-1} and 500–600cm^{-1} were noted on the HA-containing scaffold (Figure 4). These bands reportedly correspond to the presence of PO_4 in the scaffold after HA mineralization [19, 51]. Broadening of the peak at 950 cm^{-1} and superposition of 1085cm^{-1} peaks (see Figure 4) have also been attributed to the interaction of HA and chitosan [51].

Successfully engineered tissue constructs will physicochemically and structurally mimic the native tissue and its unique mechanical properties. While electrospun scaffolds morphologically resemble the fibrous structure of the ECM, the mechanical properties of fibrous scaffolds make them less suitable for use as bone analogs. Crosslinking can enhance the mechanical properties of the constructs and fine-tune them to approximate the fibrous tensile properties of bone ECM. Here we used genipin (GP) as a natural, increasingly popular non-toxic crosslinker [28, 29, 31]. Genipin-crosslinking has recently been shown to increase the mechanical strength of electrospun chitosan fibers, as inferred from suture pullout strength tests [52]. While the mechanism of how genipin crosslinks chitosan is still under investigation, a recent study suggests that this process entails a spontaneous reaction between genipin and the NH_2 subunits on the chitosan chain, which might lead to the observed increase in the scaffold stiffness. In our hands, the Young's modulus of our scaffolds increased significantly upon cross-linking, while the ultimate tensile strength was only marginally increased (Figures 6A and B). Since the mechanical properties of our scaffolds increased with HA concentrations up to 1.0% but not beyond that, we focused on 1.0% HA as a working concentration for other subsequent studies. In this study we tested our scaffolds while wet to mimic the aqueous environment of the human body. Upon crosslinking with GP, the Young's modulus of these scaffolds increased about 4-fold to 142±13 MPa, which approximates the modulus of non-weight-bearing bone.

Our findings contrast those of Zhang et al. (2010), who recently reported that incorporation of HA reduces the mechanical strength of their electrospun chitosan/collagen scaffolds [20].

The Young's modulus of their non-crosslinked chitosan/PEO scaffolds was 92.2 ± 19.1 MPa and decreased to 57.3 ± 15.5 MPa and 48.2 ± 8.3 MPa upon incorporation of HA and HA/collagen respectively. In our experiments, the Young's' modulus of 1.0% HA non-crosslinked, waterproofed chitosan scaffolds was 25.2±9.2 MPa (Figure 6B). The lower values for our scaffolds may reflect the absence of PEO or, alternatively, be due to a dispersion of the HA nanoparticles on/near the surface of the nanofibers rather than an incorporation into the molecular structure of the polymer solution. If the HA particles are in fact incorporated into the molecular structure, they will disrupt molecular chains and therefore decrease its mechanical strength. This decrease would not occur if HA is simply dispersed on or near the surface of the scaffolds. Another explanation is the substantial reduction in the amount of HA we used as compared to Zhang et. al. 2010. Our w/w% of HA and chitosan in solution is 14% HA nanoparticles with 86% CTS, whereas Zhang et. al. used 27.8% HA nanoparticles, 7.2% collagen and 57.8% CTS. This incorporation of double the amount of HA we used may have caused further disruption in the formation of stable CTS, nanofibers, causing a significant decrease in the Young' modulus. Finally, as yet another explanation, the difference in mechanical properties of the scaffolds may also be due to the fact that Zhan et al. used collagen, which is more elastic than chitosan.

In terms of functional tissue engineering, our aim was to fabricate a scaffold with structural and mechanical properties similar to those of non-load bearing bone that entail the regenerative capacity of periosteum. Specifically, our goal was to generate a bioactive scaffold capable of inducing/accelerating osteogenic differentiation similar to what occurs when osteoprogenitor cells from the periosteum migrate to the damaged bone tissue. The periosteum plays a central role in the health of bone tissue, as it is the source and site for the recruitment of osteoprogenitor cells responsible for the initiation of repair and regeneration at sites of injury [8, 53, 54]. In comparing the effects of ablating different sources of osteoprogenitor cells, recent studies showed that removal of progenitor cells from the bone marrow had minimal effect of osteogenesis, while removal of the periosteum caused a 73% decrease in new bone formation, indicating the crucial role of periosteum in regeneration [53, 54]. The osteogenic properties of our CTS-GP and CTS-HA-GP fibrous scaffolds were assessed *in vitro* using 7F2 mouse osteoblast like cells. As seen in Figure 7, the cells attach to the scaffolds, proliferate and over a 14-day period cover the scaffold in a multilayered fashion. At the same time, the metabolic activity (as inferred from AB fluorescence) decreased over time in cells cultured on HA-containing scaffolds (Figure 8B). Cells undergoing differentiation cease proliferation leads to a decrease in their metabolic activity [55]. Hence, the decrease in AB fluorescence in our study is likely due to differentiation of cells, and corresponds to the increase in ALP activity seen in Figure 8A. AB fluorescence is commonly used, upon calibration, to measure cell proliferation; a decrease in AB fluorescence is often interpreted as decreases in cell numbers [56]. However, in combination with the SEM images of proliferating cells in Figures 7A–D we surmise that decrease in AB fluorescence genuinely reflect a decrease in the metabolic activity of cells, which plateaued before reaching confluence on CTS-GP and declined on CTS-HA-GP scaffolds. We believe that this decrease is not due to cell death, but rather is a result of the cells undergoing enhanced differentiation in response to the osteogenic cues of the scaffolds (Figures 7 and 8). More recently, Venugopal et al. (2011) showed that the presence of HA in chitosan scaffolds caused a significant increase in matrix mineralization [57], further supporting our conclusion that decreased AB activity might reflect enhanced osteoblast differentiation.

In line with previous studies, ALP activity at days 7 and 14 was significantly higher ($p < 0.05$, see Figure 8A), when the cells were cultured on HA-containing bio-composite scaffolds, as compared to both CTS-GP scaffolds and TCP [18, 20]. These data suggest that both the surface topography of the substrate and the innate biochemical cues in the scaffolds may play important roles in the osteogenic maturation process. The decrease in ALP activity

by day 21 may be attributed to the further maturation of the 7F2 cells. ALP expression is reportedly higher at early stages of osteoblast differentiation peaking around days 14 or 15 [18, 20, 58]. In line with this notion, our study showed a decrease in ALP expression at day 21, indicating that maturation has progressed as also inferred from the upregulation in the expression of some of the later markers, such as osteopontin (OP), an extracellular structural protein responsible for mineralization of the ECM, and osteonectin (ON), a post-proliferative glycoprotein responsible for binding differentiated osteoblasts to the calcium found in the fully mineralized ECM, [59]. As seen in Figures 8C and D, while both CTS-GP and CTS-HA-GP scaffolds promote 7F2 cell maturation and differentiation, the cells cultured on the HA-containing scaffolds matured at a faster rate, evident by a sharp increase in ON and sharp decrease in OP mRNA from day 1 to day 14 on CTS-HA-GP scaffolds, as compared to the more gradual and linear increase on CTS-GP scaffolds ($p < 0.01$). Our data are in line with previous studies demonstrating that chitosan scaffolds support osteogenesis of pre-mature osteoblasts and the osteogenic differentiation of human bone marrow derived mesenchymal stem cells (MSC) [60–63]. For example, chitosan nanofibers -reinforced poly(butylene succinate) microfibers induced osteogenic differentiation of human bone marrow derived MSC, as assessed by by the increased gene expression of ALP, OP, bone sialoprotein, osteocalcin, Runx2 and Osterix [57]. Similarly, chitosan containing poly(caprolactone) nanofibers promoted osteogenic maturation of MC3T3 mouse preosteoblasts over a 14 day period, as assessed from the enhanced gene expression of collagen 1 and OP in the presence of chitosan when compared to TCP and PCL alone [59]. In adding to this body of evidence for the usefulness of chitosan as base material for bone scaffolds, our study is the first to show that the presence of HA and crosslinking with GP significantly enhances the mechanical strength of electrospun CTS based nanofibrous scaffolds and their capacity to induce osteogenic differentiation of osteoprogenitor cells

5. CONCLUSION

In this work we developed a simple, one-step technology to generate electrospun and HA-containing fibrous chitosan scaffolds that are subsequently crosslinked with genipin as potential substitutes for periosteum. Crosslinking with genipin resulted in five-fold increase in the Young's modulus approximating those of periosteum. Osteoinductive bioactivity of the scaffolds was demonstrated *in vitro* using 7F2 osteoblast-like cells. Based on these results, we propose that electrospun crosslinked HA-containing chitosan nanofibrous scaffolds cross-linked with genipin are potential candidates for non-weight bearing bone tissue engineering, for example for cranial and maxillofacial reconstruction. Future studies will focus on evaluating the capacity of these scaffolds to induce osteogenic differentiation in human bone marrow derived mesenchymal stem cells as well as their capabilities to repair craniofacial lesions in animal models.

Acknowledgments

This study was supported in part by grants from the National Science Foundation [grants # 0907572 (UKGW, CS and PIL) and 0434108 (PIL, MEF)], the National Institute of Diabetes and Digestive and Kidney Diseases [DK088402-03 (GPB, PIL)], the Stein Family Foundation (PIL, PL), and the Surgical Engineering Enterprise (PIL, AK), a Strategic Initiative of Drexel University College of Medicine (Drexel Med). We gratefully acknowledge the advice and materials characterization facilities provided by Dr. Karen Winey at the Materials Science Department at the University of Pennsylvania and Drs. Ed Basgill and Nikoli Zhorro at the Centralized Research Facility (CRF) at Drexel University. We also acknowledge Dr. Qingwei Zhang and Ms. Gozde Senel-Ayaz for their help with the SEM, as well as Dr. Kenneth Barbee and Dr. Allison Andrews for their help with the AFM.

Abbreviations

AB	Alamar Blue

ALP	Alkaline phosphatase
CTS	Chitosan
CTS-GP	Chitosan fibers crosslinked with genipin
CTS-HA-GP	Chitosan-hydroxyapatite fibers crosslinked with genipin
ECM	Extracellular Matrix
GP	Genipin
HA	Hydroxyapatite
ON	Osteonectin
OP	Osteopontin
PCL	Poly(caprolactone)
PEO	Poly(ethylene oxide)
PLGA	poly(lactic-co-glycolic acid)
TFA	Trifluoroacetic acid

REFERENCES

1. Banwart JC, Asher MA, Hassanein RS. Iliac crest bone graft harvest donor site morbidity. A statistical evaluation. Spine (Phila Pa 1976). 1995; 20:1055–1060. [PubMed: 7631235]
2. Borden M, Attawia M, Khan Y, Laurencin CT. Tissue engineered microsphere-based matrices for bone repair: design and evaluation. Biomaterials. 2002; 23:551–559. [PubMed: 11761175]
3. Ransford AO, Morley T, Edgar MA, Webb P, Passuti N, Chopin D, et al. Synthetic porous ceramic compared with autograft in scoliosis surgery. A prospective, randomized study of 341 patients. J Bone Joint Surg Br. 1998; 80:13–18. [PubMed: 9460945]
4. Veis A. Phosphoproteins from teeth and bone. Ciba Found Symp. 1988; 136:161–177. [PubMed: 3068008]
5. Shi S, Kirk M, Kahn AJ. The role of type I collagen in the regulation of the osteoblast phenotype. J Bone Miner Res. 1996; 11:1139–1145. [PubMed: 8854250]
6. Boskey AL, Posner AS. Bone structure, composition, and mineralization. Orthop Clin North Am. 1984; 15:597–612. [PubMed: 6387574]
7. Allen MR, Hock JM, Burr DB. Periosteum: biology, regulation, and response to osteoporosis therapies. Bone. 2004; 35:1003–1012. [PubMed: 15542024]
8. Zhang X, Awad HA, O'Keefe RJ, Guldberg RE, Schwarz EM. A perspective: engineering periosteum for structural bone graft healing. Clin Orthop Relat Res. 2008; 466:1777–1787. [PubMed: 18509709]
9. Cai YZ, Wang LL, Cai HX, Qi YY, Zou XH, Ouyang HW. Electrospun nanofibrous matrix improves the regeneration of dense cortical bone. J Biomed Mater Res A. 2010; 95:49–57. [PubMed: 20740600]
10. Woo KM, Jun JH, Chen VJ, Seo J, Baek JH, Ryoo HM, et al. Nano-fibrous scaffolding promotes osteoblast differentiation and biomineralization. Biomaterials. 2007; 28:335–343. [PubMed: 16854461]
11. Ito Y, Hasuda H, Kamitakahara M, Ohtsuki C, Tanihara M, Kang IK, et al. A composite of hydroxyapatite with electrospun biodegradable nanofibers as a tissue engineering material. J Biosci Bioeng. 2005; 100:43–49. [PubMed: 16233849]
12. Kim HW, Lee HH, Knowles JC. Electrospinning biomedical nanocomposite fibers of hydroxyapatite/poly(lactic acid) for bone regeneration. J Biomed Mater Res A. 2006; 79:643–649. [PubMed: 16826596]

13. Venugopal J, Low S, Choon AT, Sampath Kumar TS, Ramakrishna S. Mineralization of osteoblasts with electrospun collagen/hydroxyapatite nanofibers. J Mater Sci Mater Med. 2008; 19:2039–2046. [PubMed: 17957448]

14. Zhang YZ, Su B, Ramakrishna S, Lim CT. Chitosan nanofibers from an easily electrospinnable UHMWPEO-doped chitosan solution system. Biomacromolecules. 2008; 9:136–141. [PubMed: 18078323]

15. Pramanik N, Mishra D, Banerjee I, Maiti TK, Bhargava P, Pramanik P. Chemical synthesis, characterization, and biocompatibility study of hydroxyapatite/chitosan phosphate nanocomposite for bone tissue engineering applications. Int J Biomater. 2009; 2009:512417. [PubMed: 20130797]

16. Bhattarai N, Edmondson D, Veiseh O, Matsen FA, Zhang M. Electrospun chitosan-based nanofibers and their cellular compatibility. Biomaterials. 2005; 26:6176–6184. [PubMed: 15885770]

17. Prasitsilp M, Jenwithisuk R, Kongsuwan K, Damrongchai N, Watts P. Cellular responses to chitosan in vitro: the importance of deacetylation. J Mater Sci Mater Med. 2000; 11:773–778. [PubMed: 15348059]

18. Zhang Y, Venugopal JR, El-Turki A, Ramakrishna S, Su B, Lim CT. Electrospun biomimetic nanocomposite nanofibers of hydroxyapatite/chitosan for bone tissue engineering. Biomaterials. 2008; 29:4314–4322. [PubMed: 18715637]

19. Kumirska J, Czerwicka M, Kaczynski Z, Bychowska A, Brzozowski K, Thoming J, et al. Application of spectroscopic methods for structural analysis of chitin and chitosan. Mar Drugs. 2010; 8:1567–1636. [PubMed: 20559489]

20. Zhang Y, Reddy VJ, Wong SY, Li X, Su B, Ramakrishna S, et al. Enhanced biomineralization in osteoblasts on a novel electrospun biocomposite nanofibrous substrate of hydroxyapatite/collagen/chitosan. Tissue Eng Part A. 2010; 16:1949–1960. [PubMed: 20088700]

21. Thomas V, Dean DR, Jose MV, Mathew B, Chowdhury S, Vohra YK. Nanostructured biocomposite scaffolds based on collagen coelectrospun with nanohydroxyapatite. Biomacromolecules. 2007; 8:631–637. [PubMed: 17256900]

22. Teng SH, Lee EJ, Park CS, Choi WY, Shin DS, Kim HE. Bioactive nanocomposite coatings of collagen/hydroxyapatite on titanium substrates. J Mater Sci Mater Med. 2008; 19:2453–2461. [PubMed: 18219556]

23. Chen H, Huang J, Yu J, Liu S, Gu P. Electrospun chitosan-graft-poly (epsilon - caprolactone)/poly (epsilon-caprolactone) cationic nanofibrous mats as potential scaffolds for skin tissue engineering. Int J Biol Macromol. 2011; 48:13–19. [PubMed: 20933540]

24. Xie D, Huang H, Blackwood K, MacNeil S. A novel route for the production of chitosan/poly(lactide-co-glycolide) graft copolymers for electrospinning. Biomed Mater. 2010; 5:065016. [PubMed: 21079284]

25. Bat E, Kothman BH, Higuera GA, van Blitterswijk CA, Feijen J, Grijpma DW. Ultraviolet light crosslinking of poly(trimethylene carbonate) for elastomeric tissue engineering scaffolds. Biomaterials. 2010; 31:8696–8705. [PubMed: 20739060]

26. Chen ZG, Wang PW, Wei B, Mo XM, Cui FZ. Electrospun collagen-chitosan nanofiber: a biomimetic extracellular matrix for endothelial cell and smooth muscle cell. Acta Biomater. 2010; 6:372–382. [PubMed: 19632361]

27. Fathima NN, Dhathathreyan A, Ramasami T, Kragel J, Miller R. Degree of crosslinking of collagen at interfaces: adhesion and shear rheological indicators. Int J Biol Macromol. 2011; 48:67–73. [PubMed: 20932859]

28. Zhang K, Qian Y, Wang H, Fan L, Huang C, Yin A, et al. Genipin-crosslinked silk fibroin/hydroxybutyl chitosan nanofibrous scaffolds for tissue-engineering application. J Biomed Mater Res A. 2010; 95:870–881. [PubMed: 20824649]

29. Bispo VM, Mansur AA, Barbosa-Stancioli EF, Mansur HS. Biocompatibility of nanostructured chitosan/ poly(vinyl alcohol) blends chemically crosslinked with genipin for biomedical applications. J Biomed Nanotechnol. 2010; 6:166–175. [PubMed: 20738071]

30. Barbir A, Michalek AJ, Abbott RD, Iatridis JC. Effects of enzymatic digestion on compressive properties of rat intervertebral discs. J Biomech. 2010; 43:1067–1073. [PubMed: 20116063]

31. Solorio L, Zwolinski C, Lund AW, Farrell MJ, Stegemann JP. Gelatin microspheres crosslinked with genipin for local delivery of growth factors. J Tissue Eng Regen Med. 2010; 4:514–523. [PubMed: 20872738]
32. Li WJ, Laurencin CT, Caterson EJ, Tuan RS, Ko FK. Electrospun nanofibrous structure: a novel scaffold for tissue engineering. J Biomed Mater Res. 2002; 60:613–621. [PubMed: 11948520]
33. Hsieh HJ, Hsieh CY, Tsai SP, Ho MH, Wang DM, Liu CE, et al. Analysis of freeze-gelation and cross-linking processes for preparing porous chitosan scaffolds. Carbohyd Polym. 2007; 67:124–132.
34. Lelkes, PI.; Samet, MM.; Christensen, CW.; Amrani, DL. Factitious Angiogenesis: Endothelialization of Artificial Cardiovascular Prostheses. In: Maragoudakis, ME.; Gullino, PM.; Lelkes, PI., editors. Angiogenesis in Health and Disease. New York: Plenum Press; 1992. p. 339-351.
35. Raub CB, Suresh V, Krasieva T, Lyubovitsky J, Mih JD, Putnam AJ, et al. Noninvasive assessment of collagen gel microstructure and mechanics using multiphoton microscopy. Biophys J. 2007; 92:2212–2222. [PubMed: 17172303]
36. O'Brien J, Wilson I, Orton T, Pognan F. Investigation of the Alamar Blue (resazurin) fluorescent dye for the assessment of mammalian cell cytotoxicity. Eur J Biochem. 2000; 267:5421–5426. [PubMed: 10951200]
37. Hunt, M. Real Time PCR. In: Medicine UoSCSo. , editor. Microbiology and Immunology Online. Columbia: Board of Trustees of the University of South Carolina; 2010. Procedure for calculating mRNA expression and normalizing logarithmically to GAPDH and Tissue Culture Plastic Controls.
38. Desai NP, Hubbell JA. Surface Physical Interpenetrating Networks of Poly(Ethylene-Terephthalate) and Poly(Ethylene Oxide) with Biomedical Applications. Macromolecules. 1992; 25:226–232.
39. Li M, Guo Y, Wei Y, MacDiarmid AG, Lelkes PI. Electrospinning polyaniline-contained gelatin nanofibers for tissue engineering applications. Biomaterials. 2006; 27:2705–2715. [PubMed: 16352335]
40. Han J, Lazarovici P, Pomerantz C, Chen X, Wei Y, Lelkes PI. Co-Electrospun Blends of PLGA, Gelatin, and Elastin as Potential Nonthrombogenic Scaffolds for Vascular Tissue Engineering. Biomacromolecules. 2010
41. Li M, Mondrinos MJ, Chen X, Lelkes PI. Electrospun blends of natural and synthetic polymers as scaffolds for tissue engineering. Conf Proc IEEE Eng Med Biol Soc. 2005; 6:5858–5861. [PubMed: 17281592]
42. Saad FA, Hofstaetter JG. Proteomic analysis of mineralising osteoblasts identifies novel genes related to bone matrix mineralisation. Int Orthop. 2011; 35:447–451. [PubMed: 20556378]
43. Burchardt H. The biology of bone graft repair. Clin Orthop Relat Res. 1983:28–42. [PubMed: 6339139]
44. Catledge SA, Clem WC, Shrikishen N, Chowdhury S, Stanishevsky AV, Koopman M, et al. An electrospun triphasic nanofibrous scaffold for bone tissue engineering. Biomed Mater. 2007; 2:142–150. [PubMed: 18458448]
45. Schiffman JD, Schauer CL. Cross-linking chitosan nanofibers. Biomacromolecules. 2007; 8:594–601. [PubMed: 17291083]
46. Lin L, Perets A, Har-El YE, Varma D, Li M, Lazarovici P, et al. Alimentary 'green' proteins as electrospun scaffolds for skin regenerative engineering. J Tissue Eng Regen Med. 2012
47. Austero MS, Donius AE, Wegst UG, Schauer CL. New crosslinkers for electrospun chitosan fibre mats. I. Chemical analysis. Journal of the Royal Society, Interface / the Royal Society. 2012
48. Geng X, Kwon OH, Jang J. Electrospinning of chitosan dissolved in concentrated acetic acid solution. Biomaterials. 2005; 26:5427–5432. [PubMed: 15860199]
49. Cai ZX, Mo XM, Zhang KH, Fan LP, Yin AL, He CL, et al. Fabrication of Chitosan/Silk Fibroin Composite Nanofibers for Wound-dressing Applications. Int J Mol Sci. 2010; 11:3529–3539. [PubMed: 20957110]

50. Heinemann C, Heinemann S, Bernhardt A, Worch H, Hanke T. Novel textile chitosan scaffolds promote spreading, proliferation, and differentiation of osteoblasts. Biomacromolecules. 2008; 9:2913–2920. [PubMed: 18771318]
51. Danilchenko SN, Kalinkevich OV, Pogorelov MV, Kalinkevich AN, Sklyar AM, Kalinichenko TG, et al. Characterization and in vivo evaluation of chitosan-hydroxyapatite bone scaffolds made by one step coprecipitation method. J Biomed Mater Res A. 2011; 96:639–647. [PubMed: 21268238]
52. Norowski PA, Mishra S, Adatrow PC, Haggard WO, Bumgardner JD. Suture pullout strength and in vitro fibroblast and RAW 264.7 monocyte biocompatibility of genipin crosslinked nanofibrous chitosan mats for guided tissue regeneration. J Biomed Mater Res A. 2012
53. Zhang X, Xie C, Lin AS, Ito H, Awad H, Lieberman JR, et al. Periosteal progenitor cell fate in segmental cortical bone graft transplantations: implications for functional tissue engineering. J Bone Miner Res. 2005; 20:2124–2137. [PubMed: 16294266]
54. Tiyapatanaputi P, Rubery PT, Carmouche J, Schwarz EM, O'Keefe RJ, Zhang X. A novel murine segmental femoral graft model. J Orthop Res. 2004; 22:1254–1260. [PubMed: 15475206]
55. Moore KA, Lemischka IR. Stem cells and their niches. Science. 2006; 311:1880–1885. [PubMed: 16574858]
56. Mandal BB, Kundu SC. Cell proliferation and migration in silk fibroin 3D scaffolds. Biomaterials. 2009; 30:2956–2965. [PubMed: 19249094]
57. Venugopal JR, Giri Dev VR, Senthilram T, Sathiskumar D, Gupta D, Ramakrishna S. Osteoblast mineralization with composite nanofibrous substrate for bone tissue regeneration. Cell biology international. 2011; 35:73–80. [PubMed: 20923413]
58. Sasmazel HT. Novel hybrid scaffolds for the cultivation of osteoblast cells. Int J Biol Macromol. 2011; 49:838–846. [PubMed: 21839769]
59. Mostafa NZ, Uludag H, Varkey M, Dederich DN, Doschak MR, El-Bialy TH. In vitro osteogenic induction of human gingival fibroblasts for bone regeneration. The open dentistry journal. 2011; 5:139–145. [PubMed: 21915227]
60. Martins A, Pinho ED, Correlo VM, Faria S, Marques AP, Reis RL, et al. Biodegradable nanofibers-reinforced microfibrous composite scaffolds for bone tissue engineering. Tissue Eng Part A. 2010; 16:3599–3609. [PubMed: 20666612]
61. Lahiji A, Sohrabi A, Hungerford DS, Frondoza CG. Chitosan supports the expression of extracellular matrix proteins in human osteoblasts and chondrocytes. J Biomed Mater Res. 2000; 51:586–595. [PubMed: 10880106]
62. Yang X, Chen X, Wang H. Acceleration of osteogenic differentiation of preosteoblastic cells by chitosan containing nanofibrous scaffolds. Biomacromolecules. 2009; 10:2772–2778. [PubMed: 19743842]
63. Mohammadi Y, Soleimani M, Fallahi-Sichani M, Gazme A, Haddadi-Asl V, Arefian E, et al. Nanofibrous poly(epsilon-caprolactone)/poly(vinyl alcohol)/chitosan hybrid scaffolds for bone tissue engineering using mesenchymal stem cells. The International journal of artificial organs. 2007; 30:204–211. [PubMed: 17417759]

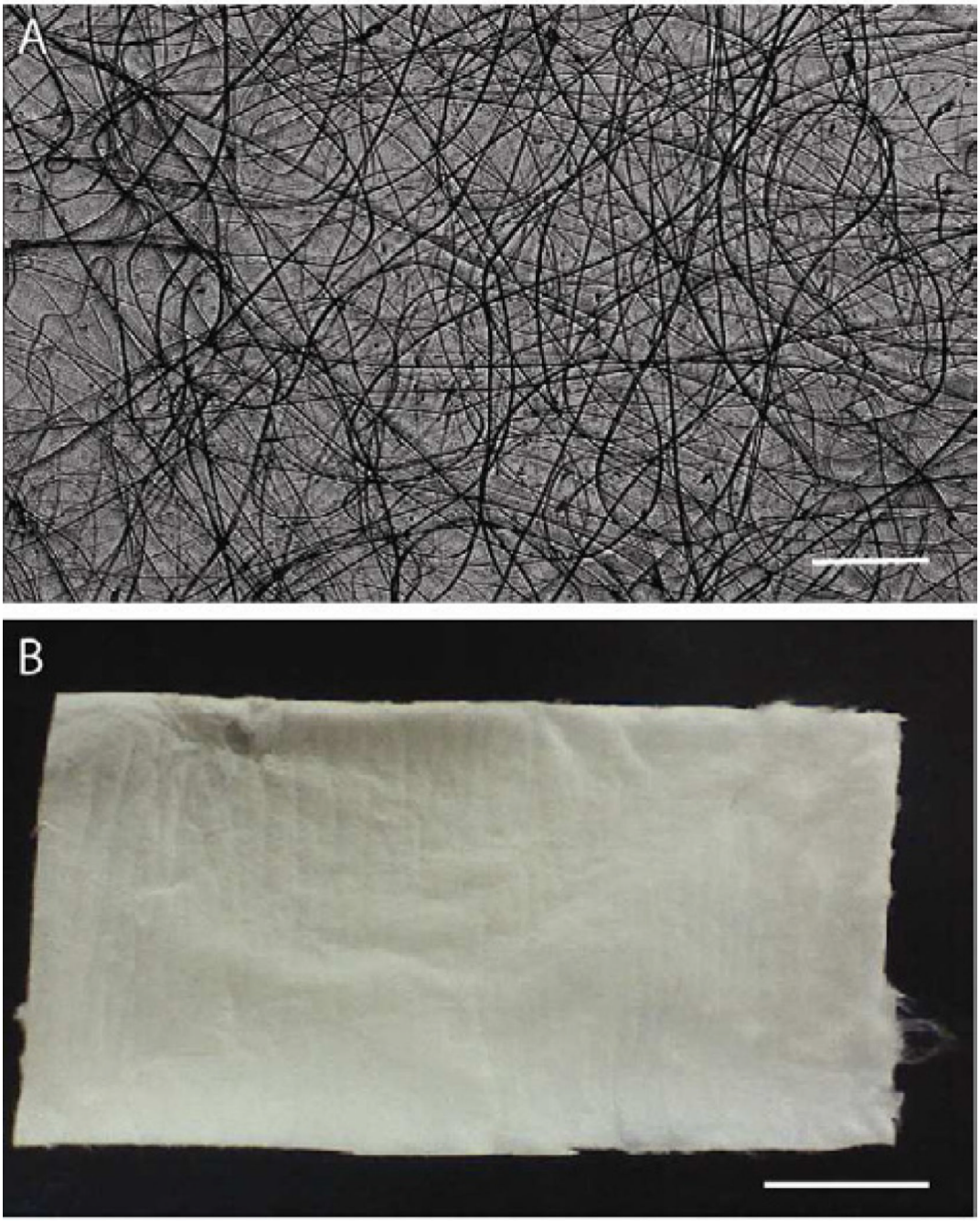

Figure 1. Macro/microscopic images of electrospun CTS fibers

Examples of electrospun chitosan microfibers (A) and of a fibrous mat (B). Scale bar for (A) is 200μm and for (B) is 1cm.

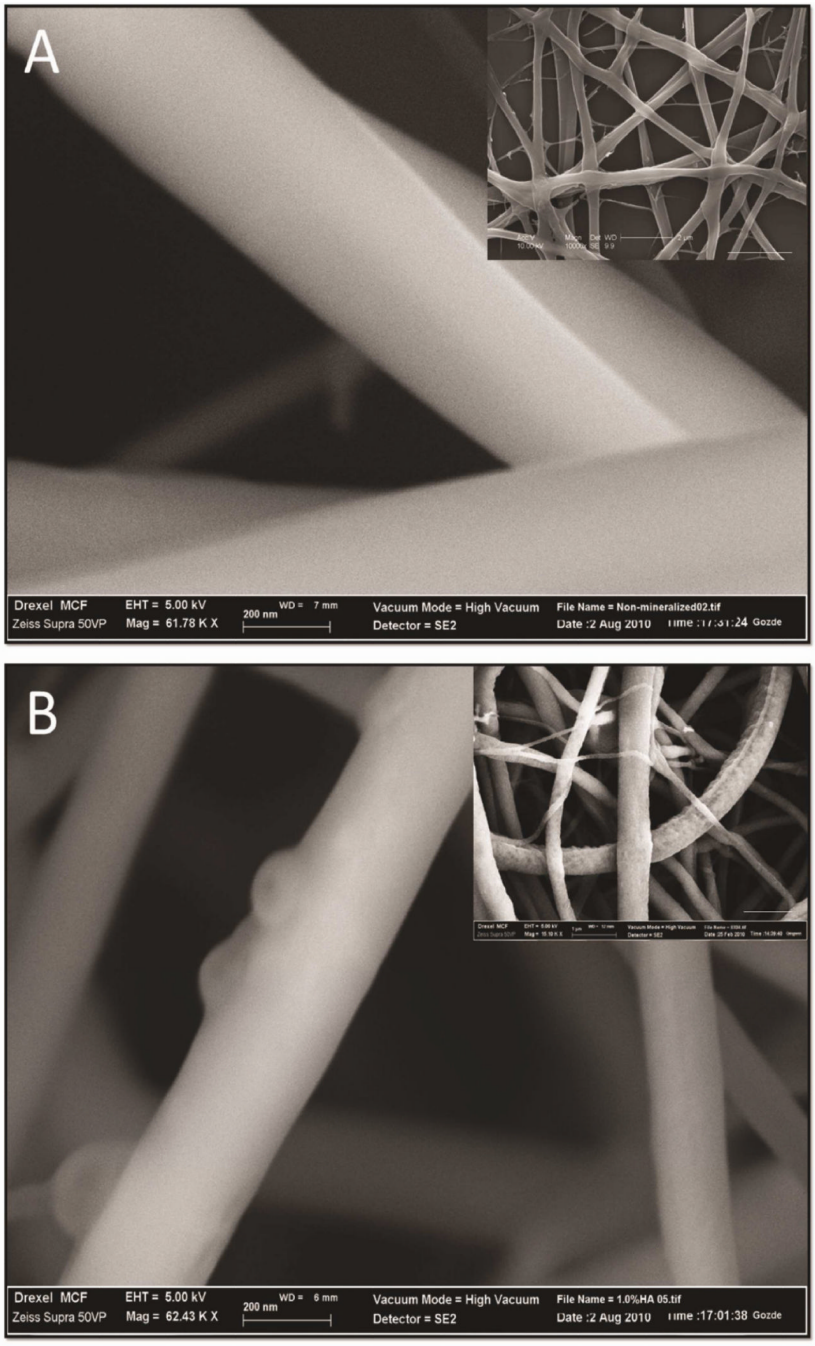

Figure 2. The morphology of electrospun scaffolds evaluated by scanning electron and atomic force microscopy

Scanning electron micrographs of 0.1% genipin crosslinked CTS-GP (A) and 0.1% genipin crosslinked 1.0% HA-containing (B) 7% chitosan nanofibers. Scale bars are 200nm. Inserts: Typical morphologies of nanofibers at lower magnification (scale bar for insert in A is 2μm and in B is 1μm).

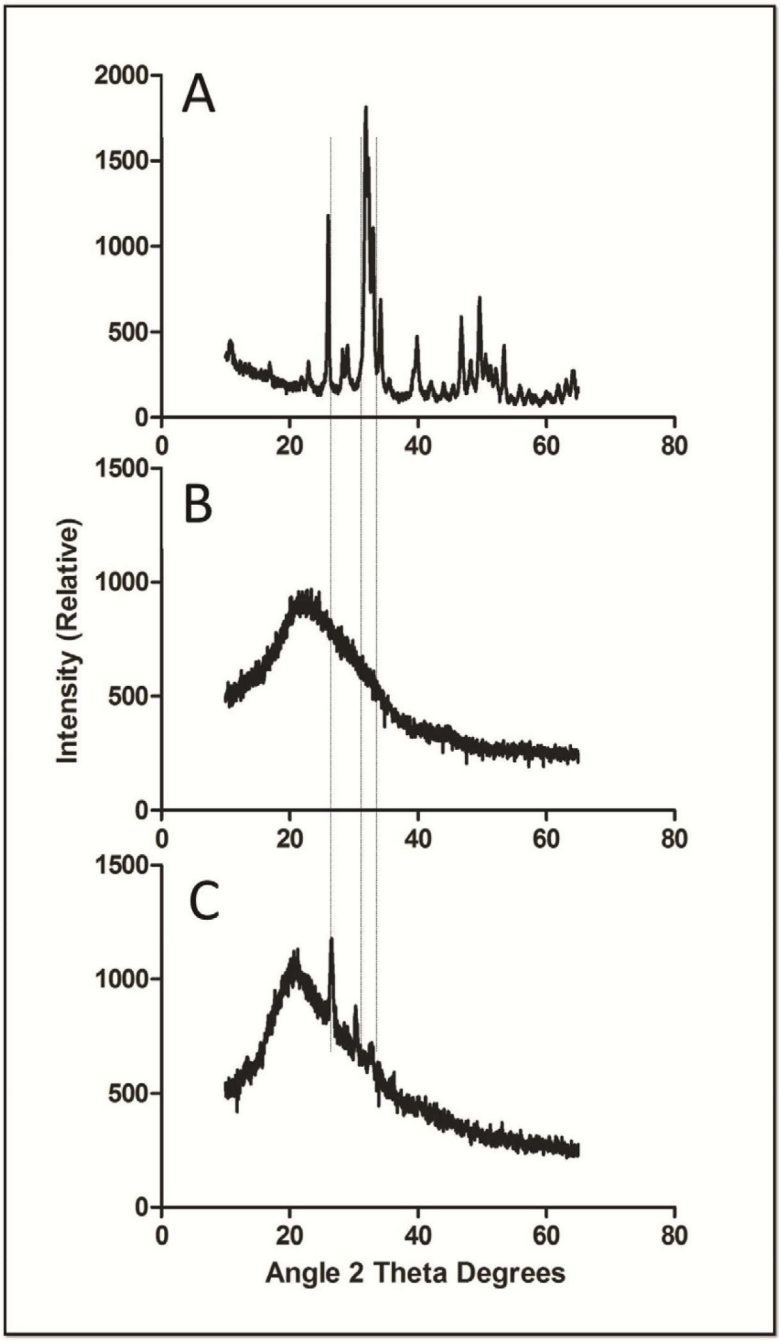

Figure 3. X-ray diffraction spectra of hydroxyapatite (A), 0.1% genipin crosslinked 7% chitosan nanofibers (B) and 1.0% HA-containing 0.1% genipin crosslinked 7% chitosan nanofibers (C)
The alignment of the peaks is indicated by the dashed lines.

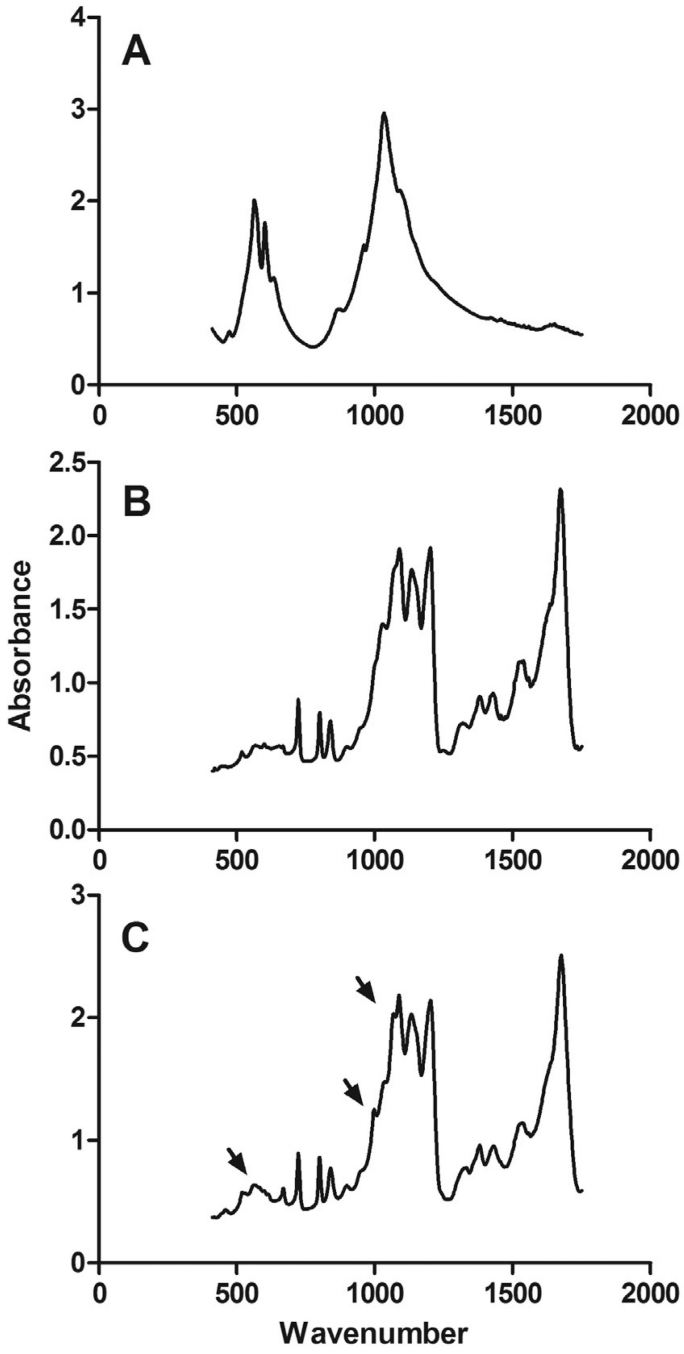

Figure 4. Fourier transform infrared spectra of hydroxyapatite (A), 0.1% genipin crosslinked 7% chitosan nanofibers (B) and 1.0% HA-containing 0.1% genipin crosslinked 7% chitosan nanofibers (C)

Peaks of interests are designated by arrows.

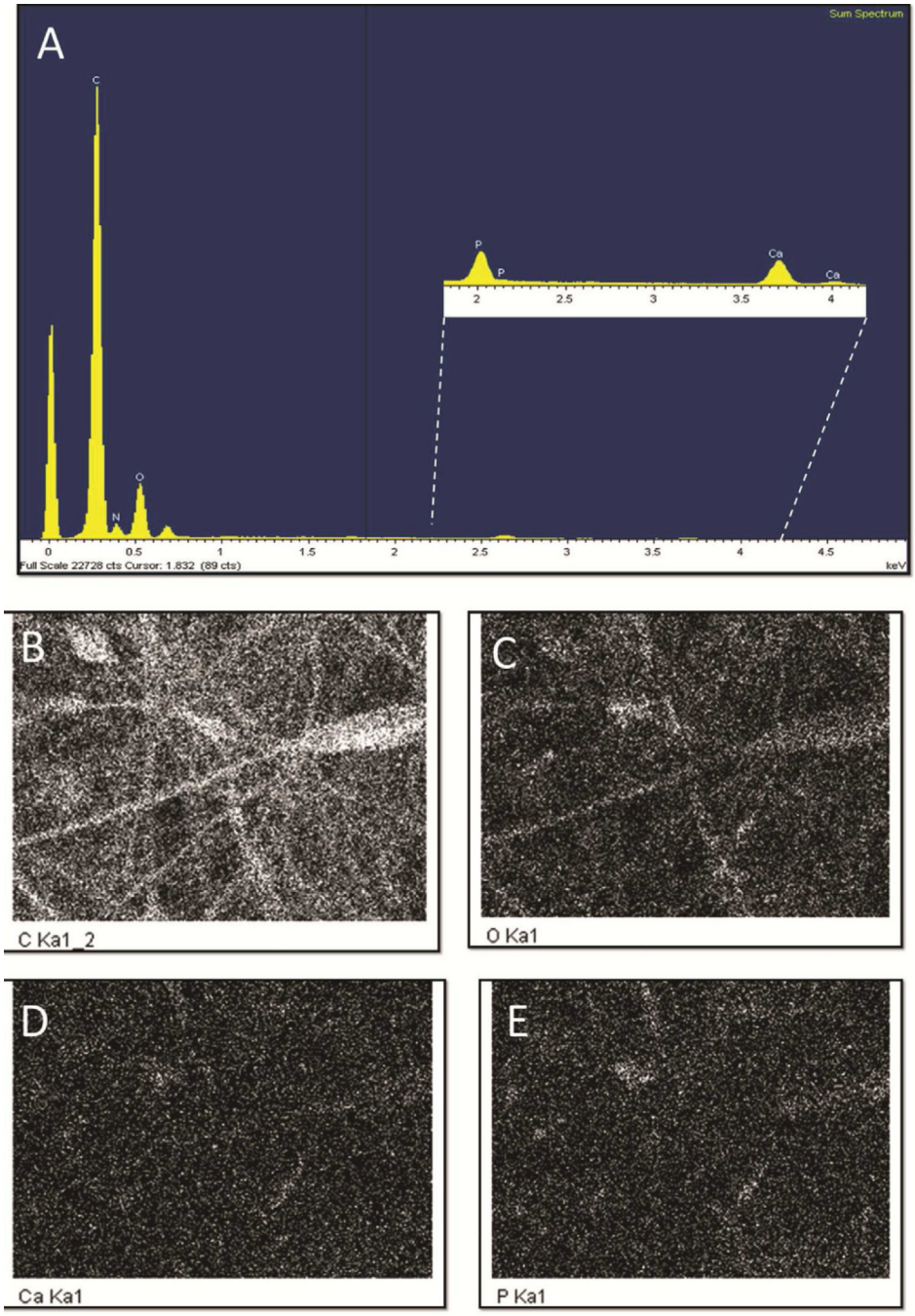

Figure 5. Electron dispersion spectroscopy of CTS-GP and CTS-HA-GP bio-composite nanofibers

Spectral analyses comparing the elemental compositions of 0.1% genipin crosslinked chitosan nanofibers (A). Insert: 1.0% HA-containing 0.1% genipin crosslinked 7% chitosan nanofibers show new peaks for calcium and phosphorous due to the presence of hydroxyapatite nanoparticles. Dot-analyses representing the elemental topographical distribution of carbon (B), oxygen (C), calcium (D) and phosphorous (E) of the HA-containing nanofibers.

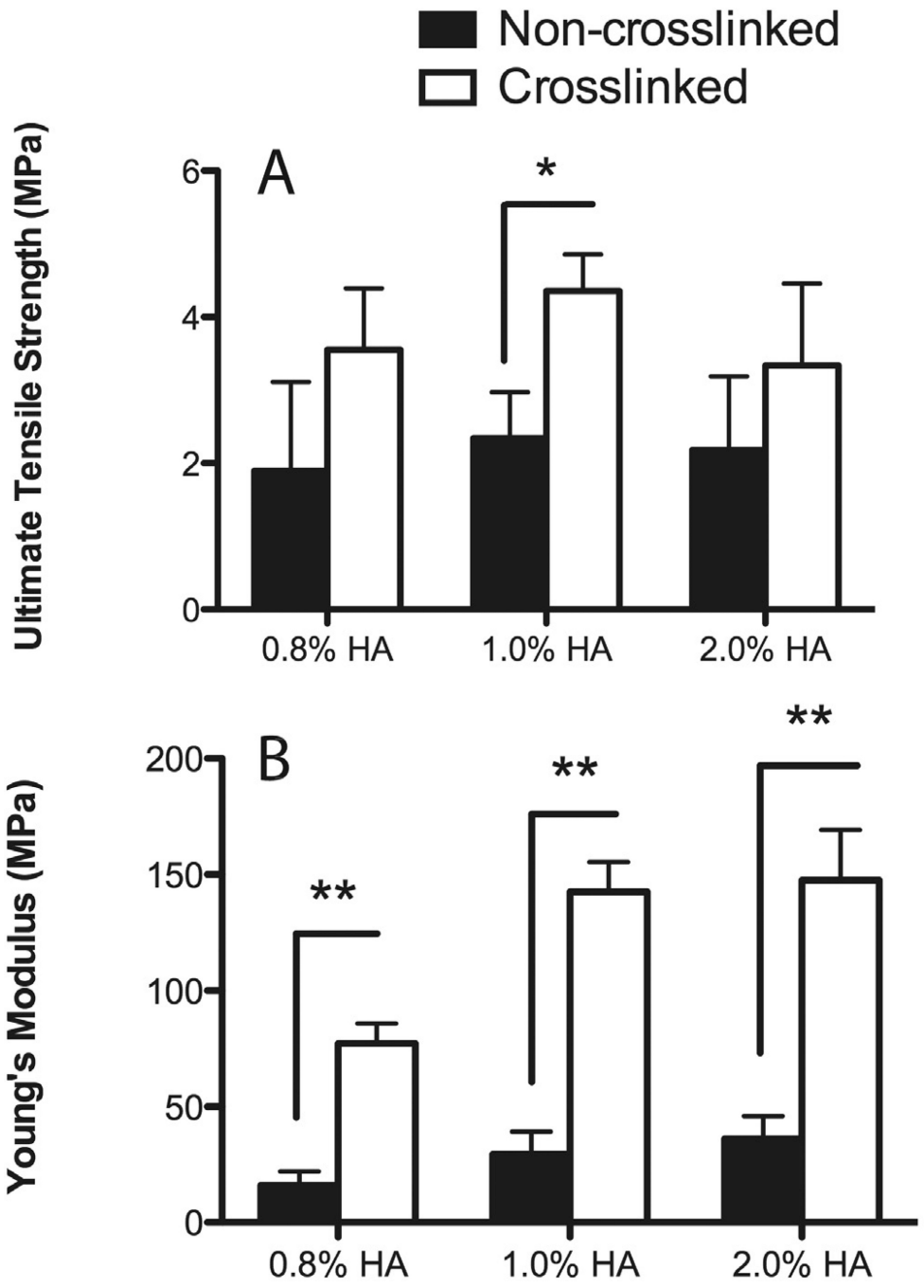

Figure 6. Ultimate Tensile Strength (A) and Young's moduli (B) of non-crosslinked (black bars 0.1% genipin and crosslinked (white bars) 7% chitosan nanofibers at different concentrations of hydroxyapatite

** indicates statistical significance at $p<0.01$ by one way ANOVA with Tukey test.

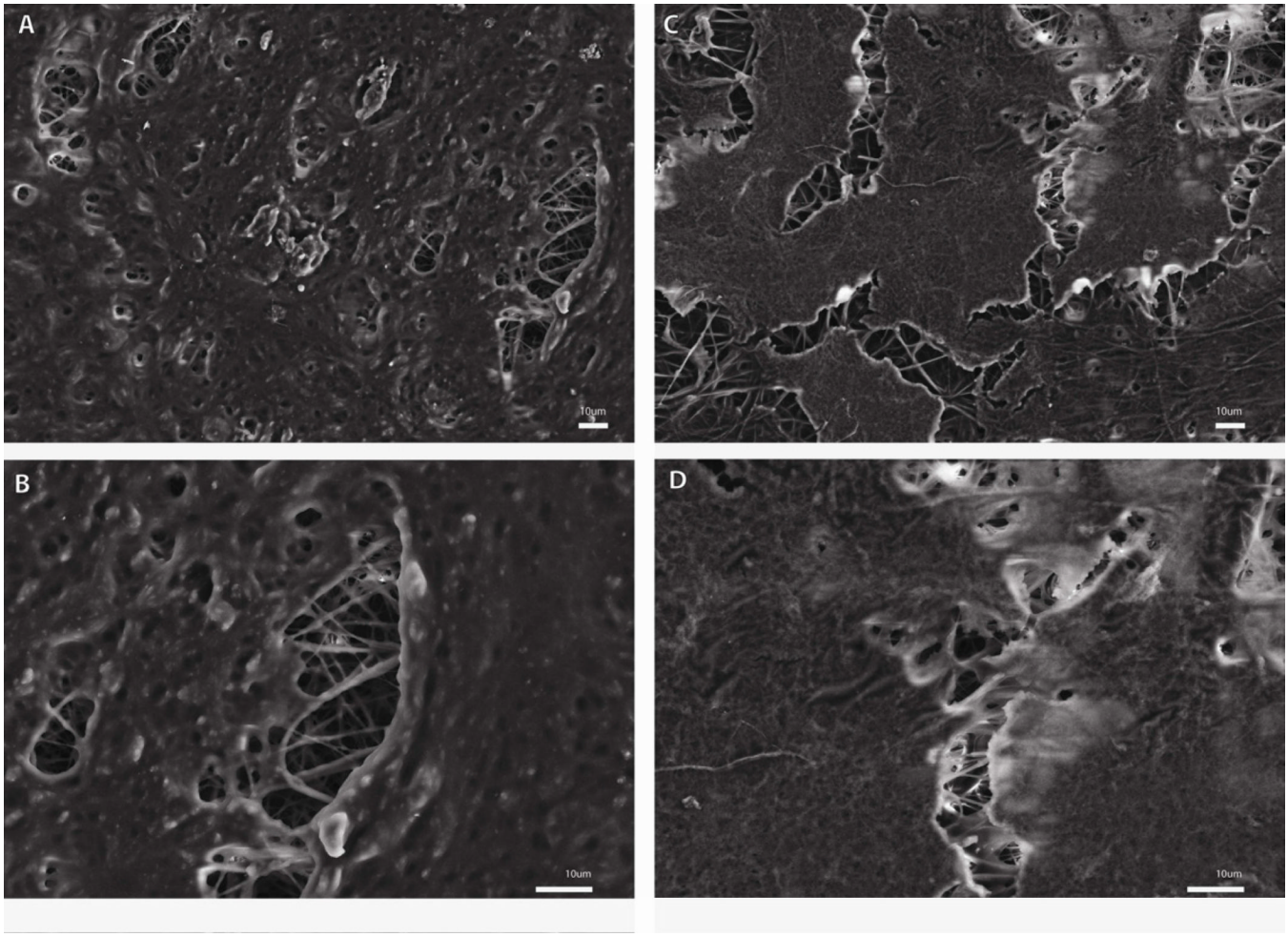

Figure 7. SEM imaging of 7F2 osteoblasts on CTS-GP and CTS-HA-GP nanofibers

SEM micrographs of 7F2 cells on CTS-GP scaffolds (A 500X and B 1000X) and CTS-HA-GP scaffolds (C 500X and D 1000X) at day 14.

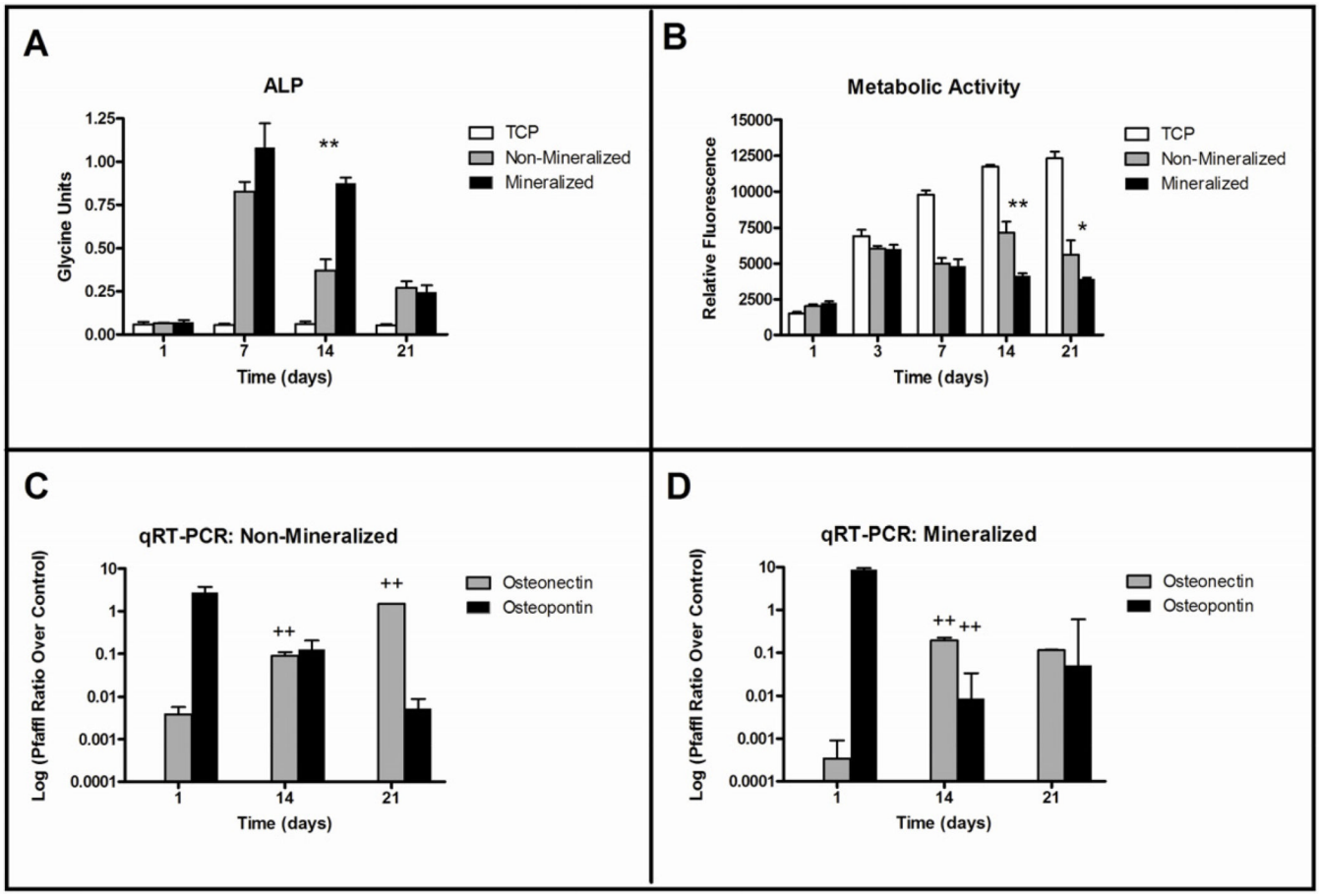

Figure 8. Metabolic activity, alkaline phosphatase expression and osteogenic marker expression of 7F2 osteoblasts on CTS-GP and CTS-HA-GP composite nanofibers

Alkaline phosphatase expression of 7F2 osteoblasts on days 1, 7, 14 and 21 (A), metabolic activity of 7F2 osteoblasts measured by alamar blue on days 1, 3, 7, 14 and 21 and mRNA expression of osteopontin and osteonectin of 7F2 osteoblasts on days 1, 14 and 21 on CTS-GP (C) and CTS-HA-GP (D) 0.1% genipin crosslinked chitosan nanofibers. * and ** indicate a significant difference ($p < 0.05$ and $p < 0.01$ respectively) between CTS-GP and CTS-HA-GP scaffolds at the same time point; ++ indicates a significant difference ($p < 0.01$) of the specified scaffold compared to the same scaffolds at the earlier time point.